TOMCAT: A beamline for TOmographic Microscopy and Coherent rAdiology experimenTs

M. Stampanoni, A. Groso, A. Isenegger, G. Mikuljan, Q. Chen, D. Meister, M. Lange, R. Betemps, S. Henein and R. Abela

Swiss Light Source, Paul Scherrer Institut, CH-5232 Villigen, Switzerland

Abstract. Synchrotron-based X-ray Tomographic Microscopy (SRXTM) is nowadays a powerful technique for non-destructive, high-resolution investigations of a broad kind of materials. High-brilliance and high-coherence third generation synchrotron radiation facilities allow micrometer and sub-micrometer, quantitative, three-dimensional imaging within very short time and extend the traditional absorption imaging technique to edge-enhanced and pure phase-sensitive measurements. At the Swiss Light Source, a new, tomography dedicated beamline called TOMCAT has been recently build. The new beamline get photons from a 2.9 T superbend with a critical energy of 11.1 keV. This makes energies above 20 keV easily accessible. To guarantee the best beam quality (stability and homogeneity), the number of optical elements has been kept to a minimum. A Double Crystal Multilayer Monochromator (DCMM) covers an energy range between 8 and 45 keV with a bandwidth of a few percent down to 10^{-4}. The beamline can also be operated in white-beam mode, providing the ideal conditions for real-time coherent radiology.

Keywords: X-ray imaging, synchrotron microtomography, coherent radiology
PACS: 07.85.Qe, 81.70.Tx, 07.85.Tt

INTRODUCTION

Microtomographic investigations tend nowadays towards the analysis of millimeter-sized specimens at micrometer resolution within minutes. The combination of X-ray microscopy with tomographic techniques as well as the exceptional properties of third-generation synchrotron radiation sources allow to obtain volumetric information of a specimen at micron or sub-micron scale with minimal sample preparation. In addition, the coherent nature of synchrotron radiation extends the classical absorption based tomography towards edge-enhanced and phase-contrast investigations. The requirements on the detectors in terms of spatial resolution and efficiency are therefore very high and tremendous efforts have been made all over the world to develop synchrotron-based microtomography devices. The most established detection method consists of converting X-rays into visible light with a scintillator and projecting them onto a charge coupled device (CCD) with the help of suitable optics [1, 2, 3, 4]. This approach provides reliable and reproducible results for a wide range of research fields covering both medicine and biology [5, 6, 7, 8] as well as materials science [9, 10, 11]. Even thought almost the totality of today's routine users usually performs absorption-based or "edge-enhanced" tomography experiments, there is a growing interest on pure phase contrast imaging. The advantages of X-ray phase contrast radiography over conventional radiography are evident. First, the phase shift of light absorbing materials can be sufficiently big to be detected with phase-sensitive methods and, second, phase signals are produced with much lower dose deposition than absorption, which can be very important when radiation damage becomes an issue. It has been shown that interferometric techniques as proposed by Bonse and Hart [12], or phase retrieval methods[13] work fine but are somehow difficult to use in a routine experiment because of their complexity (stability and alignment issues for the first one, data post-processing for the second one). Recently, two new methods have been introduced which set a novel approach to the phase contrast problem: the Differential Phase Contrast (DPC) technique [14] and the Modified Bronnikov Algorithm (MBA) [15, 16]. The DPC is based on a combination of grid-interferometry and phase stepping and is particularly suited for large objects and when a moderate resolution is required. The MBA is based on fast and direct 3D approach and works perfectly when micrometer resolution is necessary and the samples are small. It appears clear that the development potential of micron- and submicron tomography applications, in absorption or in phase, are far to be fully exploited. The Swiss Light Source (SLS) and its TOMCAT beamline will be at the forefront in this context.

THE TOMCAT BEAMLINE

The TOMCAT beamline is located at the X02DA port of the SLS. Synchrotron light is delivered by a 2.9 T superbend, see Figure 2a. Compared with the 1.4 T of the normal SLS bending magnets this shifts the critical energy of the source from 5.4 keV up to 11.1 keV. This results in a considerable increase of flux at hard X-rays ($>$ 20 keV), see Figure 1.

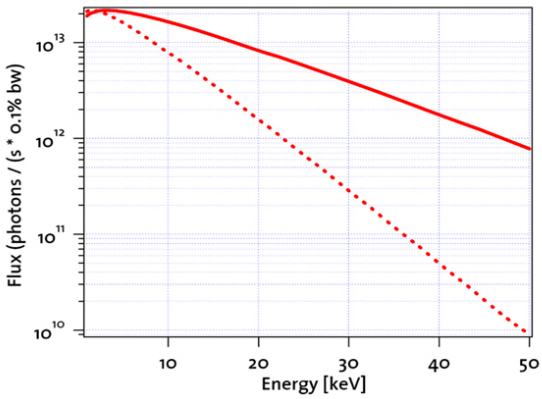

Machine Parameters	
Ring energy	2.4 GeV
Ring current	400 mA
Source parameters	
Magnetic field	2.9 T
Critical energy	11.1 keV / 1.12 Å
Electron source size (σ_x, σ_y)	46 μm, 16 μm
Electron source divergence (σ'_x, σ'_y)	109 μrad,16 μrad
Photon source size (Σ_x, Σ_y)	53 μm, 16 μm
Photon source divergence (Σ'_x, Σ'_y)	2 mrad, 0.6 mrad

FIGURE 1. Left: estimated photon flux (vertical integrated and 2 mrad horizontal acceptance) for the 2.9 T superbend (full line) and for the 1.4 T normal bend (dashed line). The gain at energies above 20 keV is evident. Right: Relevant parameters of the source. The vertical divergence is, of course, energy dependent. The value of 0.6 mrad correponds to the acceptance of the beamline diaphragm.

Design and realization

Rationale. Real space, full field imaging, and in particular tomography, needs a homogeneous beam profile, in order to perform optimal background corrections. Because of the high coherence of the radiation produced by third-generation synchrotron radiation facilities like the SLS, all the optical components (windows, mirrors and monochromator) must be designed with particular care in order to avoid deterioration of the beam profile. The design criteria for the optics of the TOMCAT beamline have been:

- Keep the optics as simple as possible (i.e. minimize the number of optical elements)
- Optimize optics for bandwidth either than for energy resolution
- Monochromatic beam and white beam must be available
- Energy range: at least 8-40 keV

Window. The machine UHV-sector (10^{-10} mbar) is separated from the beamline HV (10^{-7} mbar) by a Chemical Vapour Deposited (CVD) diamond window, see Figure 2b. Because of their better surface-roughness, CVD diamond windows are preferred to standard Be-windows. The thickness of the window is 100 μm and its surface-roughness 2.5 nm RMS. Coherence degradation due to the window has been measured with shearing interferometry[17] and resulted to be negligible.

Optics. The main optical component of the TOMCAT beamline is a fixed-exit double crystal multilayer monochromator (DCMM) which covers an energy range from 6 to 45 keV. The DCMM is located in the front-end, at approximately 7 m from the source: this allows to accept a large angular divergence while keeping the optical elements very compact. $[Ru/C]_{100}$ and a $[W/Si]_{100}$ multilayer stripes have been coated 8 mm apart from each other on a Si111 substrate (active area of 150x50 mm^2), Figure 2c. As a results the energy bandwidth of the DCMM is a few percent when multilayer are used or 10^{-4} when the silicon is used. The slope errors figures in the direction along and across the optic are better than 0.5 μrad RMS and 5 μrad RMS respectively. Surface roughness is less than 0.3 nm RMS. When operating with multilayers the Bragg angle varies from $\theta_B = 1.82^\circ$ and $\theta_B = 0.265^\circ$ for energies ranging from 5 keV up to 45 keV. For the low-energy settings, the power density is 80 mW/mm^2 and is dissipated via a water side-cooling.

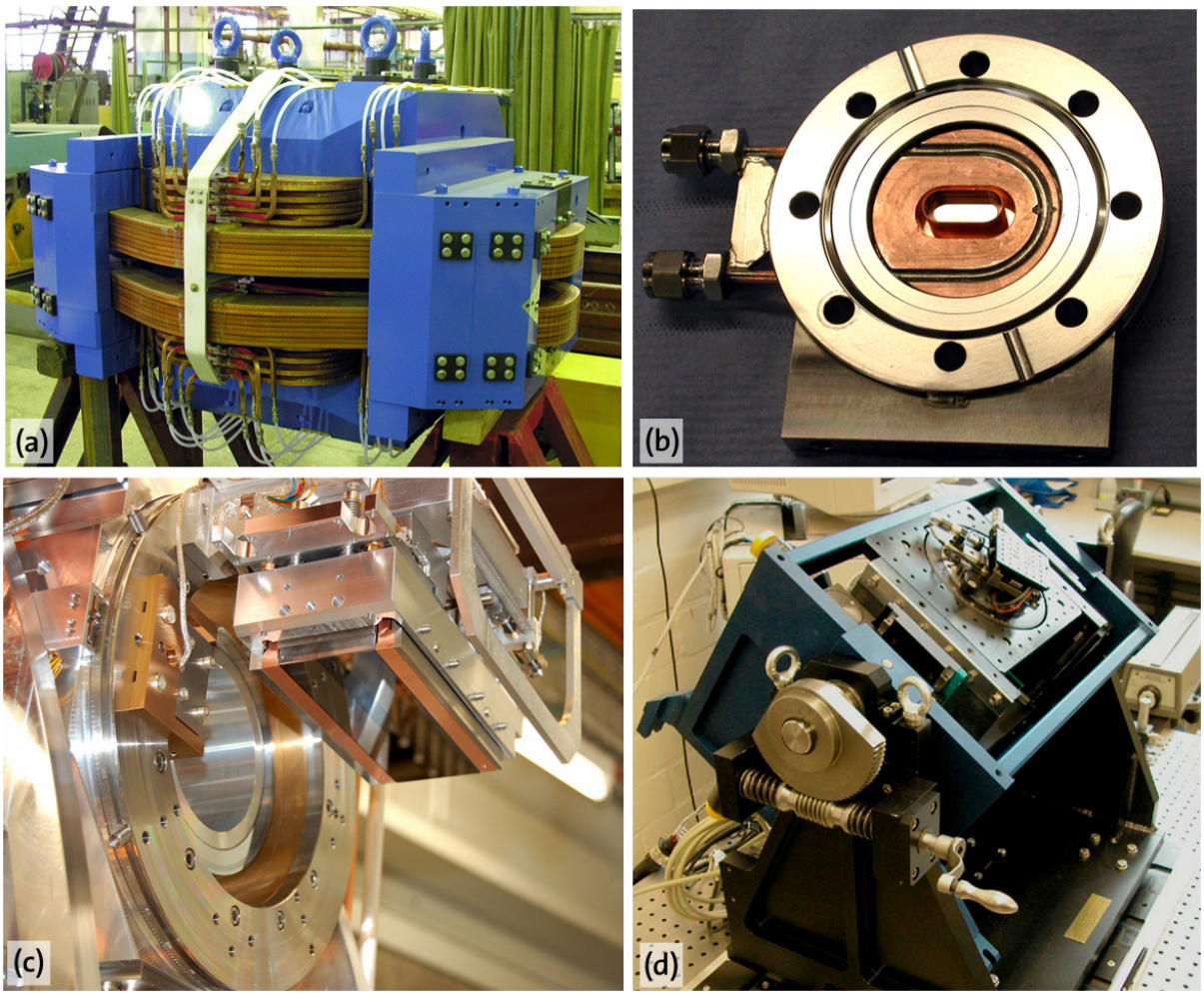

FIGURE 2. (a) The 2.9 T superbend before the installation in the ring. (b) The CVD window installed in the front end: clearly visible is the copper frame, which is water cooled. (c) Multilayer crystals installed on one goniometer of the TOMCAT monochromator. Visible are the three ($[Ru/C]_{100}$, $[W/Si]_{100}$ and Si111) regions on the substrate. (d) The sample manipulator "frozen" during the axis swapping procedure.

The crystal optics are mounted on two independent high-precision goniometers. The first crystal has motorized pitch, roll, and horizontal translation (for stripes selection); the second crystal has the same degrees of freedom and, in addition, yaw and vertical translation. The whole system is positioned on a base plate that can be vertically adjusted. The distance between both crystals can be increased up to 850 mm. There is no additional mirror and, therefore, the vertical size of the beam is "controlled" by moving the endstation along the beam path (up to 15 m travel range).

Sample manipulator. The sample manipulator has been designed and manufactured at PSI. Translation along all the three space direction is performed with a resolution better than 1 micron. The axis perpendicular to the beam direction has a reproducibility of 0.1 micron: this is imperative for an artefact-free acquisition of reference images. The sample can be centered also with 0.1 micron reproducibility. The rotation axis is air-bearing based and has a run-out error of less then 1 micron at 100 mm from the rotation surface. The whole system can be swapped by 90°, see Figure 2d, allowing to scan thick and short sample (vertical rotation axis) or long and thin samples (horizontal rotation axis).

Detector. X-rays are converted to visible light by a YAG:Ce or LAG:Eu thin scintillating screen. A diffraction limited microscope optics collects the light and projects the information on the CCD. With interchangeable (motorized)

objectives the field of view can easily be varied from 0.75x0.75 mm^2 up to 11.45x11.45 mm^2 with pixel sizes ranging from 0.35x0.35 μm^2 up to 5.6x5.6 μm^2. The CCD camera has 2048x2048 pixels and a full frame is read-out in 260 ms with nominal 14 bits. Readout noise is 9 e^- at 10 MHz and 12 e^- at 20 MHz, dark current is 0.022 e^-/ s/pixel.

Applications

The TOMCAT beamline will be dedicated to high-throughput microtomography experiments, providing a powerful, state-of-the-art and user-friendly instrument. Standard absorption-based techniques will be complemented by novel phase contrast based experiments. Broadband radiation will be used for real-time microradiography experiments and ultrafast tomography. Figure 3 shows some examples of the capability of the instrument.

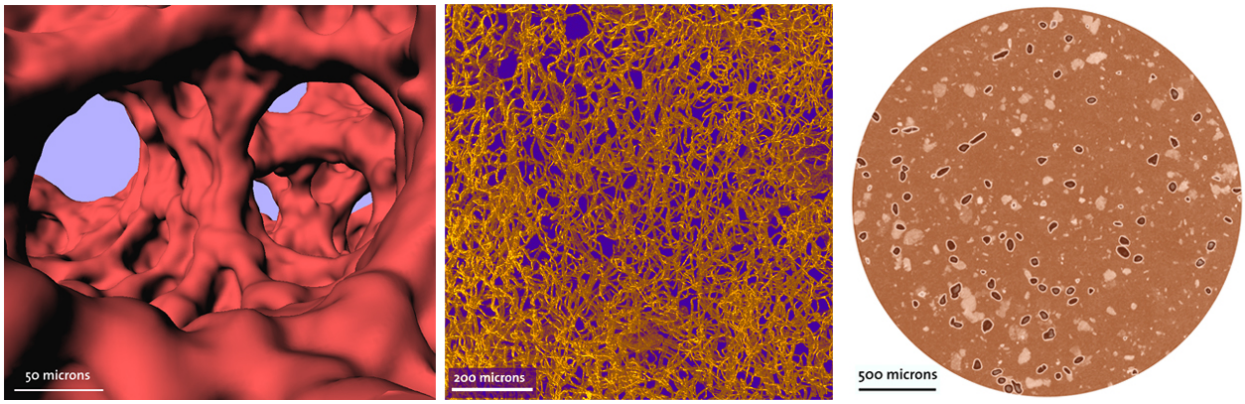

FIGURE 3. Left: surface rendering of an air cavity in a mouse lung (sample courtesy of J. Schittny, University of Bern). Center: projection view of the microvasculature structure of a monkey brain biopsy (sample courtesy of B. Weber, Max Plank Institute, Tübingen. Right: projection view of a soil sample with iodine inclusions (sample courtesy of F. Enzmann, University of Mainz).

REFERENCES

1. U. Bonse, and F. Busch, *Progress in Biophysics and Molecular Biology* **65**, 133 (1996).
2. R. Lee, B. Lai, W. Yun, D. C. Mancini, and Z. Cai, "X-Ray microtomography as a fast three-dimensional imaging technology using a CCD camera coupled with a $CdWO_4$ single-crystal scintillator," in *Developments in X-Ray Tomography*, edited by U. Bonse, 1997, vol. 3149 of *Proc. SPIE*, p. 257.
3. T. Weitkamp, C. Raven, and A. Snigierv, "An imaging and microtomography facility at the ESRF beamline ID 22," in *Developments in X-Ray Tomography II*, edited by U. Bonse, 1999, vol. 3772 of *Proc. SPIE*, p. 311.
4. M. Stampanoni, G. L. Borchert, P. Wyss, R. Abela, B. D. Patterson, S. Hunt, D. Vermeulen, and P. Rüegsegger, *Nucl. Intrum. Meth. Phys. Res. A* **491**, 291–301 (2002).
5. S. Nuzzo, F. Peyrin, P. Cloetens, J. Baruchel, and G. Boivin, *Medical Physics* **29**, 2672–2681 (2002).
6. P. Thurner, P. Wyss, R. Voide, M. Stauber, M. Stampanoni, U. Sennhauser, and R. Müller, *Bone* (2006), in press.
7. S. Heinzer, T. Krucker, M. Stampanoni, R. Abela, E. Meyer, A. Schuler, P. Schneider, and R. Müller, *Neuroimage* (2006), in press.
8. B. Müller, M. Riedel, and P. Thurner, *Microscopy and microanalysis* **12**, 97–105 (2006).
9. R. H. Mathiesen, L. Arnberg, F. Mo, T. Weitkamp, and A. Snigirev, *Physical Review Letters* **83**, 5062–5065 (1999).
10. M. Heggli, T. E. amd P. Wyss, P. J. Uggowitzer, and A. A. Gusev, *Advanced Engineering Materials* **7**, 225–229 (2005).
11. S. Waelchli, P. R. von Rohr, and M. Stampanoni, *Journal of Flow Visualization and Image Processing* **12**, 1–13 (2005).
12. U. Bonse, and M. Hart, *Applied Physics Letters.* **6**, 155–157 (1965).
13. P. Cloetens, W. Ludwig, J. Baruchel, D. V. Dyck, J. V. Landuyt, J. P. Guigay, and M. Schlenker, *Applied Physics Letters* **75**, 2912–2914 (1999).
14. T. Weitkamp, F. Pfeiffer, O. Bunk, A. Diaz, M. Stampanoni, E. Ziegler, P. Cloetens, and C. David, *Optics Express* **12**, 6296–6304 (2005).
15. A. Groso, P. Schneider, S. Linga, R. Müller, R. Abela, and M. Stampanoni, *Applied Physics Letter* (2006), in press.
16. A. Groso (2006), submitted.
17. F. Pfeiffer, O. Bunk, C. Schulze-Briese, A. Diaz, T. Weitkamp, C. David, J. F. van der Veen, I. Vartanyants, and I. K. Robinson, *Physical Review Letters* **94**, 164801–4 (2005).